A novel 25 Gbps electro-optic Pockels modulator integrated on an advanced Si photonic platform

F. Eltes[1], M. Kroh[2], D. Caimi[1], C. Mai[2], Y. Popoff[1,3], G. Winzer[2], D. Petousi[2], S. Lischke[2], J. E. Ortmann[4], L. Czornomaz[1], L. Zimmermann[2], J. Fompeyrine[1], S. Abel[1]

[1]IBM Research – Zurich, Säumerstrasse 4, 8803 Rüschlikon, Switzerland, email: fee@zurich.ibm.com,

[2]IHP, Frankfurt (Oder), Germany, [3]EMPA, Dübendorf, Switzerland, [4]The University of Texas at Austin, Austin, TX, USA

***Abstract*—** We demonstrate the first electro-optic modulator exploiting the Pockels effect, monolithically integrated on an advanced Si photonics platform. This novel technology outperforms Si photonic modulators in modulation efficiency, losses, and static tuning power. The devices, based on barium titanate thin films on 200 mm substrates, show excellent $V_\pi L$ (0.3 Vcm) and $V_\pi L\alpha$ (1.7 VdB), work at high speed (25 Gbps), and can be tuned at low static power consumption (100 nW). Our concept serves as a key building block in EPIC for next generation 100G systems.

I. Introduction

Silicon based photonic integrated circuits (PIC) are becoming a key contender for application in various areas of communication [1], and more specifically for large data center related transceivers. This technology allows for integrated optic and electronic functionality combined with advanced manufacturing, and delivers the required high-speed performance with scaling advantages in cost. Monolithic integration with electronic circuits (EPIC) is particularly important for transceiver solutions, where shrinking module footprints need dense integration of RF frontends with complex LF signal processing. Leaving aside the integration of light sources (so far mainly approached by co-packaging), it is recognized that the modulator is a critical component for systems targeting beyond 25 GBd symbol rate. The standard silicon photonic modulator implementation relies on phase shifters based on the optical carrier dispersion effect, which suffers from low overall efficiency and leads to detrimental effects such as nonlinearity, high-loss, and combined amplitude and phase modulation. Altogether these effects are known to limit the high-speed performance of silicon photonic phase shifters [2]. From the perspective of silicon transceiver technology, it would be highly desirable to have available in a silicon photonic technology pure electro-optic, i.e. Pockels, phase shifters without residual amplitude modulation, with high linearity, high efficiency and low loss. Recently, there have been many attempts to demonstrate Pockels modulators that could potentially be integrated with Si-EPIC. The most relevant approaches aim to either induce a Pockels effect in silicon via strain engineering [3], use direct wafer bonding from $LiNbO_3$ wafers [4], or introduce novel materials with large Pockels coefficients [5, 6]. All work reported so far suffers either from a weak Pockels effect [3], from incompatibility between wafer sizes [4], from thermal stability issues [6], or from incompatibility with standard Si-EPIC processes [5].

Our approach is based on single crystalline, ferroelectric $BaTiO_3$ (BTO) as a material with a large Pockels coefficient and a direct integration route with silicon [10]. Passive structures with low-propagation losses can be fabricated [11], and high-speed modulators based on BTO have already been demonstrated [12]. Excellent thermal stability has also been recently shown in BTO-based devices [13]. Following this path, we here demonstrate the integration of Pockels modulators based on BTO in an EPIC-compatible silicon photonic process flow, (E)PIC, show scalability up to 200 mm, and prove high-speed data transmission with transfer rates up to 25 Gbps.

II. Integration

Our concept of high-speed transceivers relies on the monolithic integration of BTO thin films via direct wafer bonding above an interlayer dielectric (ILD) in a standard EPIC flow (**Fig. 1**). The bonding step can be performed on top of any ILD above the FEOL structures. Mach-Zehnder modulators (MZM) for operation at 1550 nm are made from silicon strip-loaded waveguides on top of the BTO layer with lateral electrodes from the underlying metal level to provide DC and RF electric fields (**Fig. 2**). The effective electro-optic response of BTO is superior compared to alternative material systems (**Fig. 3**). It depends on the relative orientation of the BTO crystalline axes with respect to the electric switching field and to the propagation of the optical mode [10]. We maximized the response by designing BTO layers with their ferroelectric polarization in the plane of the substrate and aligning the active waveguides along the $BaTiO_3$[110] direction. Effective Pockels coefficients, r_{eff}, of ~150 pm/V have been reported for this configuration [10].

Using a process previously reported [10, 14], BTO thin films of high crystalline quality (**Fig. 4**) were epitaxially deposited on 4 nm $SrTiO_3$ buffers on silicon-on-insulator (SOI) wafers, with 100 nm top Si. Subsequently, the top Si and the BTO layer were transferred onto SiO_2 terminated host wafers via direct wafer bonding, with thin alumina layers serving as bonding interface. The excellent bonding strength yields a transfer ratio close to 100%. We successfully transferred BTO layers using 200 mm source and target wafers, confirming the scalability of our integration approach (**Fig. 5a**). X-ray diffraction analysis on 200 mm wafers after bonding reveals very good uniformity with only minimal variations in the structural characteristics along the radius of the 200 mm wafer (**Fig. 5b**). For the fabrication of modulators, we used 200 mm target wafers, processed following a (E)PIC flow having the

same back-end-of-line (BEOL) processes as EPIC runs [15]. For this work, the (E)PIC process was interrupted after 4 metallization levels, top metal 1 (TM1). After deposition and planarization of an ILD to reduce step heights and surface roughness, we transferred 170-nm-thick BTO layers from SOI wafers onto the PIC wafers. We fabricated Si waveguides, leaving the BTO layer unpatterned. An additional metallization level was added to increase the voltage drop across the BTO region, which enhances the electric field and thus the Pockels response (**Fig. 2**). Therefore, the BTO layer was etched to access the TM1 level along the strip-loaded waveguides. These openings were filled with metal to form an electrical contact between the buried RF lines and the BTO layer. An optical micrograph (**Fig. 7**) as well as a cross-sectional electron micrograph (**Fig. 8**) show the final structures after the BTO modulator integration.

III. Device Performance and Discussion

We first verified the compatibility of the BTO modulator integration process with the thermal budget restrictions imposed by the (E)PIC flow. As a low temperature method, direct wafer bonding will have very limited impact on the characteristics of pre-existing (E)PIC circuits. However, the thermal budget profile used in this work includes a long anneal step at 350ºC. Ge photodiodes (PD) were characterized before and after BTO device integration (**Fig. 9**) to ensure no influence from the thermal budget. Despite their sensitivity to thermal treatments, the measured Ge PD are unaffected by the integration flow, and confirmed the feasibility of our integration concept.

Optical simulations of the waveguide cross-section confirmed that the transverse electric (TE) mode overlaps substantially with the BTO layer. The high confinement factor of 38% enables phase modulation of the TE mode via the Pockels effect. The modeled performance of similar device structures has been reported elsewhere, and suggests excellent figure of merit compared to silicon modulators [16]. Passive ring-resonators with high Q-factors (~50'000) and low losses (5.8 dB/cm) (**Fig. 10**) confirm that the optical quality of the grown BTO layer is preserved after the full integration process. For electro-optic characterization, unbalanced MZM's (ΔL ~ 630 µm, L ~ 1-2 mm, **Fig. 11**) were used for DC as well as for RF characterization. By applying a voltage to one of the arms, we experimentally observe a shift of the transmission spectrum due to a change of the refractive index (**Fig. 12**), as expected from the Pockels effect. The electro-optic response corresponds to a $V_\pi L$ of 0.3 Vcm, which is a strong improvement compared to a typical $V_\pi L$ of ~2 Vcm for state-of-the-art Si photonics modulators [2, 17]. Taking into account the propagation losses gives a $V_\pi L\alpha$ of 1.7 VdB, significantly lower than in Si modulators (~20 VdB) [17, 18]. When sweeping the bias voltage, the phase shift of the MZM exhibited a hysteretic behavior (**Fig. 13a**), consistent with the ferroelectric nature of BTO. The hysteresis curve illustrates the need for poling the BTO layer with a bias above the coercive field (~ 1 V) to avoid a mixed domain state with vanishing r_{eff} [10] (**Fig. 13b**). Moreover, unlike the plasma dispersion effect in Si photonic modulators, the Pockels effect is not related to any current or charge injection. The measured low leakage also allows the MZM to be tuned at a low power (100 nW) (**Fig. 14**).

The small signal electrical and electro-optic bandwidth of a MZM with 1-mm-long electrodes (**Fig. 15**) shows a limited bandwidth (2 GHz). For faster RF performance, the dielectric properties of the specific materials stack, as well as parasitics coming from to the top metallization step need to be considered for further layout optimization. Modulators fabricated using ring resonators based on similar BTO/Si waveguides indeed show a cutoff frequency above 20 GHz, limited by the photonic life time in the ring-cavity (**Fig. 15**), confirming an intrinsic bandwidth in BTO higher than measured in the MZM. Data transmission experiments were done using a 1-mm-long MZM operated in single-drive mode, with a 2 V bias. Because of the low static power consumption, the bias voltage can be fine-tuned to set the quadrature point without any power consuming heaters. Eye-diagrams could be recorded at data-rates up to 25 Gbps (**Fig. 16**), which demonstrates the capability of the device to perform high-speed modulation. The metrics of the BTO devices outperform current solutions in efficiency, losses, and process compatibility (**Fig. 17**).

IV. Conclusion

We integrated barium titanate thin films with a strong Pockels coefficient into an EPIC compatible process flow. We further demonstrate the applicability of such a technology for a novel class of high-speed photonic modulators. Our results are the first example of a modulator with no fundamental road-blocks for incorporation in future 100G systems.

Acknowledgment

This project has received funding from the European Commission under grant agreement no. FP7-ICT-2013-11-619456-SITOGA, H2020-ICT-2015-25-688579 (PHRESCO), and 688282 (PETMEM), from the Swiss State Secretariat for Education, Research and Innovation under contract no. 15.0285 and 16.0001, and from the Swiss National Foundation project no 200021_159565 PADOMO.

References

[1] M. Hochberg, et al., Nat. Photonics, vol. 4, pp. 492-494, 2010. [2] D. Petousi, et al., IEEE J. Sel. Top. Quant., vol. 21, pp. 199-206, 2015. [3] M. Cazzanelli, et al., Nat. Mater., vol. 11, pp. 148-154, 2012. [4] P. Rabiei, et al., Opt. Express, vol. 21, pp. 25573-25576, 2013. [5] K. Alexander, et al., CLEO, JTh5C.7, 2017. [6] S. Koeber, et al., Light-Sci. Appl., vol. 4, p. e255, 2015. [7] J. Durel, et al., IEDM, 2016. [8] G. Reed, et al., Nat. Photonics, vol. 4, pp. 527-534, 2010. [9] D. Janner, et al., Laser Photonics Rev., vol. 3, pp. 301-313, 2009. [10] S. Abel, et al., Nat. Commun., vol. 4, p. 1671, 2013. [11] F. Eltes, et al., ACS Photonics, vol. 3, no. 9, pp. 1698-1703, 2016. [12] P. Girouard, et al., IEEE J. Quantum Elect., vol. 53, pp. 1558-1713, 2017. [13] A. Messner, F. Eltes, et al., OFC, Th5C.7, 2017. [14] R. A. McKee, et al., Phys. Rev. Lett., vol. 81, pp. 3014-3017, 1998. [15] D. Knoll, et al., IEDM, 2015. [16] P. Castera, et al., Opt. Express, vol. 23, p. 15332, 2015. [17] D. Patel, et al., Opt. Express, vol. 24, pp. 14263-14287, 2015. [18] M. Webster, et al., OFC, W4H.3, 2015. [19] S. Abel, et al., Ch. 10 in Thin Films on Silicon, World Scientific, 2016.

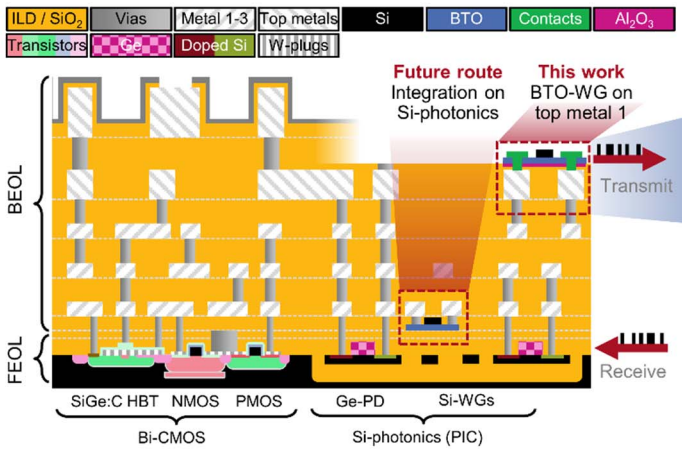

Fig. 1. Integration concept for high-speed $BaTiO_3$ electro-optic modulators. BTO layers can be integrated at any intermediate ILD level. In this work, we fabricated modulators on top of the TM1 layer. The schematics correspond to the CMOS integration scheme by IHP (simplified, not to scale).

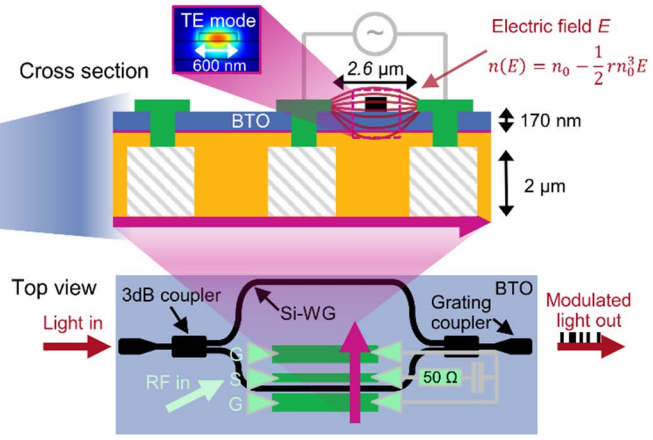

Fig. 2. Cross section and top-view of an unbalanced MZM based on the Pockels effect in a BTO thin film. The inset (top) shows the optical power distribution of the transverse electric (TE) mode in the Si/BTO waveguide. The electric field lines between the electrodes are indicated in the cross-sectional view in red.

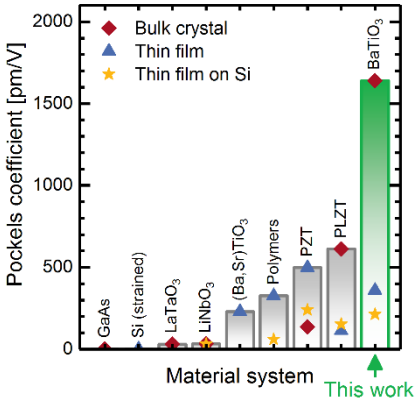

Fig. 3. Comparison of Pockels effect as reported in literature for various materials systems [19]. In this work, we focus on BTO due to the superior Pockels coefficients.

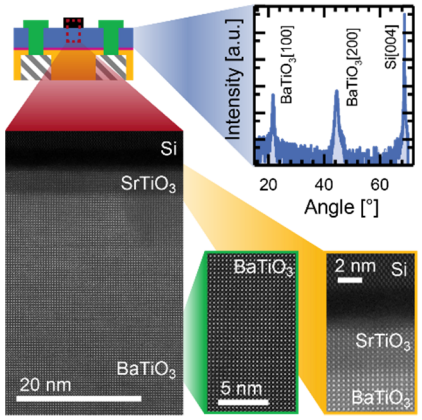

Fig. 4. HRSTEM images of BTO, showing high crystalline quality and the epitaxial relationship to Si, as confirmed by the XRD scan (top right). The images correspond to the region of the waveguides highlighted in the top left.

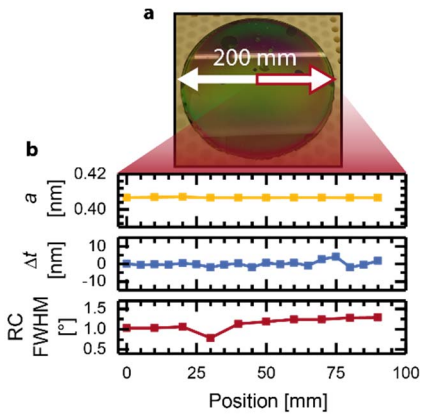

Fig. 5. (a) Photo of 200 mm wafer after BTO bonding. (b) Out-of-plane lattice constant *a*, BTO thickness variations Δt (ellipsometry), and FWHM of the rocking curve (RC) from the center to the edge of the wafer show good homogeneity.

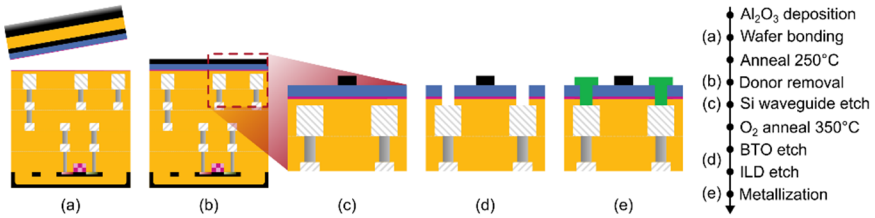

Fig. 6. Process flow for integration of BTO modulators in the BEOL of an (E)PIC process flow. Schematics of the cross sections (left) are shown at various steps in the integration process flow (right).

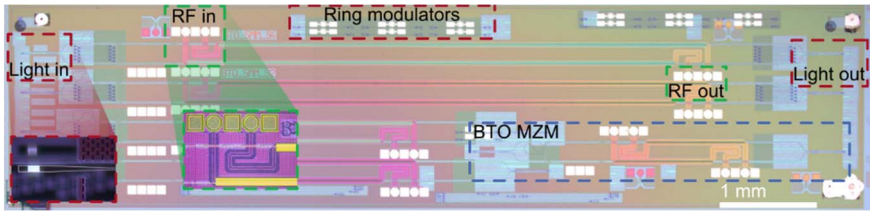

Fig. 7. Optical microscopy image (top view) of the final chip with integrated BTO. Specific devices and couplers are marked. Insets show dark-field images of highlighted areas.

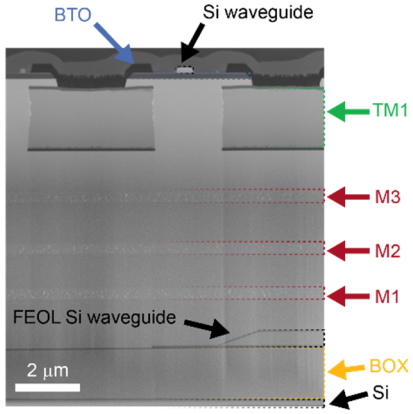

Fig. 8. Cross-sectional STEM image of BTO modulator integrated after TM1 in BEOL process on (E)PIC flow. The layers on top of the waveguide originate from the FIB sample preparation.

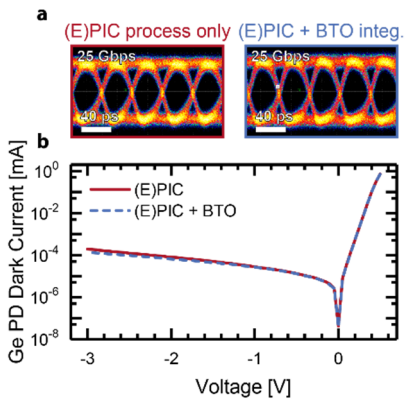

Fig. 9. Comparison of Ge PDs before and after BTO integration. The RF characteristics as visible in the eye diagrams (a) and the dark current of the photodiodes (b) are unaffected by the BTO integration process.

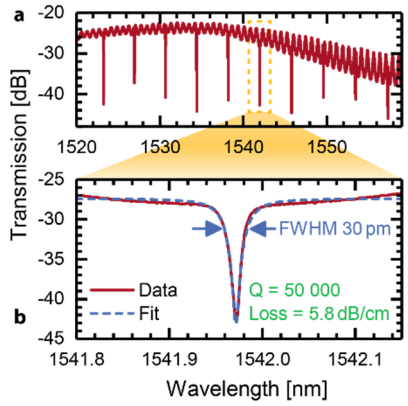

Fig. 10. Transmission spectrum of a ring resonator with radius 30 µm (a). The FWHM of the resonances is 30 pm (b), corresponding to a quality factor of 50'000 and propagation losses of 5.8 dB/cm.

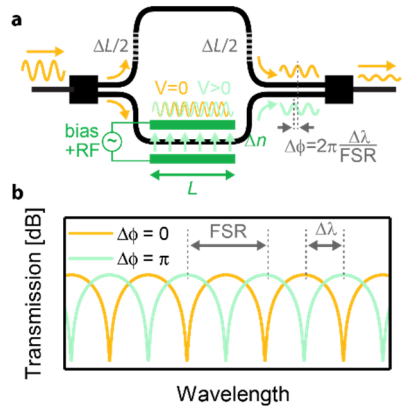

Fig. 11. Principle of an unbalanced MZM modulator using the Pockels effect. The refractive index is changed in one arm by Δn due to the Pockels effect, resulting in a relative phase shift $\Delta\Phi$ at the output (a). As a consequence, the transmission spectrum shifts by $\Delta\lambda$ (b).

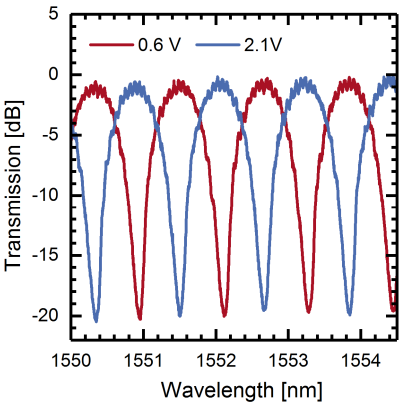

Fig. 12. Transmission spectra of MZM for different bias voltages applied to one arm of a 2-mm-long MZM, corresponding to a $V_\pi L$ of 0.3 Vcm.

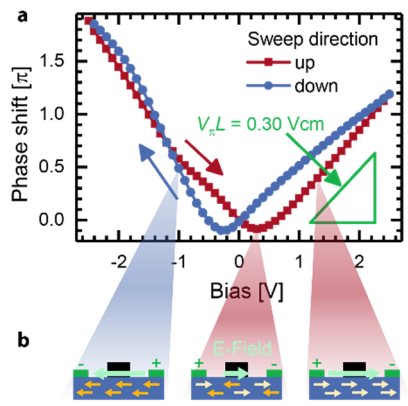

Fig. 13. (a) Induced phase shift when applying voltage to one arm of a 2-mm-long MZM. (b) The hysteretic behavior originates from domain switching in the BTO layer. The yellow arrows correspond to the polarization of ferroelectric domains.

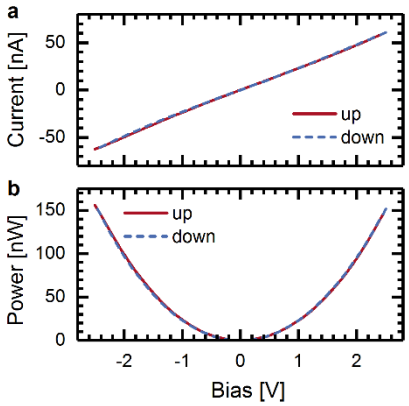

Fig. 14. Current-voltage (a) and power-voltage (b) characteristics of a 2-mm-long MZM device. The leakage current is small in the full bias range (<100 nA), resulting in low static power consumption of ~100 nW at the operating point of 2 V.

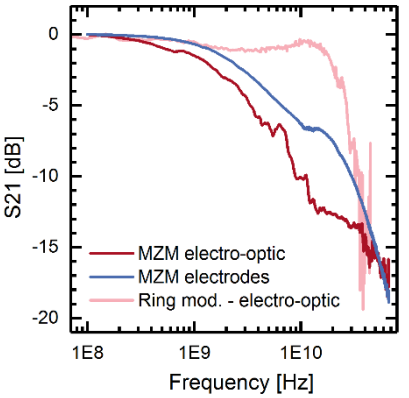

Fig. 15. Small signal frequency response of a 1-mm-long MZM and the corresponding RF electrode. The performance is mainly limited by the electrical bandwidth. A BTO/Si ring modulator with similar cross section shows a larger electro-optic bandwidth.

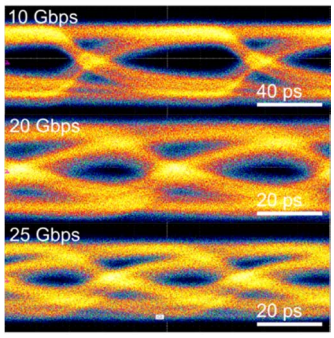

Fig. 16. Eye diagrams for data transmission through a 1-mm-long MZM in single-drive mode at 10, 20, and 25 Gbps, respectively. A bias voltage of 2 V was applied, along with a large signal modulation voltage of V_{pp} ~ 4.2 V. Accounting for electrode attenuation at 10 GHz (Fig. 15) this corresponds to a V_{pp} ~ 2 V.

	This work	[17]	[18]	[5]	[6]
Active material	**BTO**	Doped Si		PZT	Organics
$V_\pi L$ [Vcm]	**0.3**	2.8	0.2	1	0.1
$V_\pi L\alpha$ [VdB]	**1.7**	27	13	< 1	6
Poling voltage [V]	**2**	-		40	40
EPIC compatible	**YES**	YES		NO	NO

Fig. 17. Comparison of relevant FOM for state-of-the-art devices based on different electro-optic modulator technologies. The listed $V_\pi L$ values are for a single phase-shifter.